Heat Mass Transfer (2007) 44:61–70
DOI 10.1007/s00231-006-0219-2

ORIGINAL

A numerical simulation of external heat transfer around turbine blades

K. Maaroofi · M. R. H. Nobari · E. Shirani

Received: 18 March 2006 / Accepted: 1 December 2006 / Published online: 4 January 2007

Abstract External heat transfer prediction is performed in two-dimensional turbine blade cascades using the Reynolds-averaged Navier–Stokes equations. For this purpose, six different turbulence models including the algebraic Baldwin–Lomax (AIAA paper 78-257, 1978), three low-*Re* *k*–ε models (Chien in AIAA J 20:33–38, 1982; Launder and Sharma in Lett Heat Mass Transf 1(2):131–138, 1974; Biswas and Fukuyama in J Turbomach 116:765–773, 1994), and two *k*–*ω* models (Wilcox in AIAA J 32(2):247–255, 1994) are taken into account. The computer code developed employs a finite volume method to solve governing equations based on an explicit time marching approach with capability to simulate subsonic, transonic and supersonic flows. The Roe method is used to decompose the inviscid fluxes and the gradient theorem to decompose viscous fluxes. The performance of different turbulence models in prediction of heat transfer is examined. To do so, the effect of Reynolds and Mach numbers along with the turbulent intensity are taken into account, and the numerical results obtained are compared with the experimental data available.

List of symbols

c	chord length
g	blade pitch
H	heat transfer coefficient
I	angle of attack
k	turbulent kinetic energy
K, κ	Baldwin–Lomax constant
M	Mach number
P	pressure
S	coordinate along the blade profile
T	temperature
t	time
U	total velocity
x	stream wise coordinate
y	normal distance from the wall
c_p	specific heat
l_m	length scale in *k*–ε equation
Pr	Prandtl number
q_j	rate of heat transfer
Re	Reynolds number
T_u	turbulent intensity
U_i	velocity component
ε	turbulent dissipation
ω	specific dissipation
γ	specific heat ratio
ρ	density
μ	dynamic viscosity
ν	kinematics viscosity
λ	stagger angle
Ω	rotation
δ_{ij}	Kroneker delta
τ_{ij}	stress tensor

Subscripts

t	turbulent property
∞	free stream property
I	isentropic property

K. Maaroofi · M. R. H. Nobari (✉)
Department of Mechanical Engineering,
Amir Kabir University of Technology, 424 Hafez Avenue,
P.O. Box 15875-4413, Tehran, Iran
e-mail: mrnobari@cic.aut.ac.ir

E. Shirani
Department of Mechanical Engineering,
Isfahan University of Technology, Tehran, Iran

wall property at wall
1 entrance
2 exit
o stagnation property

Superscripts
lam laminar
turb turbulent

1 Introduction

The development of computational fluid dynamics (CFD) techniques in 1970s, provided excellent method for simulation of internal and external flow using the Euler and Navier–Stokes equations. Since then, numerical methods, grid generation techniques, proper ways of applying boundary conditions, data processing and more advanced computing devices has been rapidly developed and become suitable tools for CFD.

In the last decade, numerical simulation of flows and design, and analysis of the turbomachines has become common. Due to the high temperature and pressure of flow at the inlet of the gas turbines, one needs to simulate the flow numerically to calculate the heat transfer between the flow and blades and optimize the problem.

The flow in a turbine is very complex. Large pressure gradients lead to strongly accelerated and decelerated regions of flow. Under some operating conditions, there might be separated regions. The gas entering the turbine comes from a combustor and is strongly turbulent. This increase the heat transfer in the laminar and the turbulent parts [1, 2] of boundary layers. It can also cause an earlier boundary layer transition. Shocks and shock-boundary layer interaction can trigger transition or separation and affect the heat transfer. Unsteady effects, caused by wakes and shocks from the preceding stages sweeping over the blades, can increase the heat transfer significantly [3–5]. In a real turbine secondary flows and 3D effects are also important [6]. Film cooling leads to even more complications, and will not be considered here.

Simplified methods like boundary layer solvers and Navier–Stokes solvers with algebraic turbulence models have been used by many researchers in the past to predict turbine heat transfer [7–9].

This can gives good results for simple cases, but for cases with separated region, shocks and high turbulence levels, these methods often have problems. By using a full Navier–Stokes solver with a transport turbulence model it is possible to account for history affects associated with the turbulence and thereby solve or reduce the problem encountered with other simpler methods.

The main objective of this work are to simulate the flow and heat transfer around a turbine blade and compare different turbulence models used to calculate correctly the heat transfer rate. The VKI blade profile is used and H-type numerical grid is generated using an elliptic differential equation. The two-dimensional (2D) Navier–Stokes are descretized using a control volume approach and solved explicitly for flow around a 2D isothermal blade. Performance of six different turbulence models consisting of the algebraic Baldwin–Lomax [10], three low-*Re* k–ε models [1–3], and two k–ω models [4] are studied.

2 Governing equations

Two-dimensional unsteady compressible Navier–Stokes equations along with the energy equation used in this work are:

$$\frac{\partial \rho}{\partial t} + [\rho u_i]_{,j} = 0 \tag{1}$$

$$\frac{\partial (\rho u_i)}{\partial t} + \left[\rho u_i u_j + p\delta_{ij} - \tau_{ij}\right]_{,j} = 0 \tag{2}$$

$$\frac{\partial}{\partial t}(\rho e_0) + \left[(\rho e_0 + p)u_j + q_j - u_i \tau_{ij}\right]_{,j} = 0 \tag{3}$$

The fluid is assumed to be a perfect gas and the following state equation is used for pressure.

$$P = (\gamma - 1)\left(\rho e_o - \frac{1}{2}\rho u_k u_k - \rho k\right) \tag{4}$$

the shear stress tensor is

$$\tau_{ij} = \tau_{ij}^{\text{lam}} + \tau_{ij}^{\text{turb}} \tag{5}$$

where, the laminar stress tensor is

$$\tau_{ij}^{\text{lam}} = \mu\left(u_{i,j} + u_{j,i} - \frac{2}{3}u_{k,k}\delta_{ij}\right) \tag{6}$$

In addition, turbulent stress is

$$\tau_{ij}^{\text{turb}} = -\rho\overline{u_i' u_j'} = \mu_t\left(u_{i,j} + u_{i,j} - \frac{2}{3}u_{k,k}\delta_{ij}\right) - \frac{2}{3}\rho k\delta_{ij} \tag{7}$$

Similarly, the conductive heat transfer rate is

$$q_i = q_i^{\text{lam}} + q_i^{\text{turb}} \tag{8}$$

$$q_i^{\text{lam}} = -C_p \frac{\mu}{P_r} T_{,i} = \frac{-\gamma}{\gamma - 1} \frac{\mu}{P_r} \left[\frac{P}{\rho}\right]_{,i} \tag{9}$$

$$q_i^{\text{turb}} = C_p \overline{\rho T' u_i'} = -C_p \frac{\mu_t}{p_{r_t}} T_{,i} = -\frac{\gamma}{\gamma - 1} \frac{\mu_t}{p_{r_t}} \left[\frac{p}{\rho}\right]_{,i} \tag{10}$$

The fluid is assumed air and the laminar viscosity is determined through Sutherland's law: $\mu = 3.038816 \times 10^{-7} \times T^{0.72}$, where T is in Kelvin and μ is in kg/(ms). The Prandtl number is assumed 0.7 and the turbulent Prandtl number is assumed 0.9.

3 Turbulence models

Still direct numerical simulation of turbulence phenomena is not possible at high Reynolds numbers. Therefore, different turbulence models are carried out to resolve the turbulence problems. Here, six of them are considered to study the complicated flow field in a turbine cascade.

The Baldwin–Lomax model [10] is a two layer, algebraic, eddy-viscosity model that has proven to be numerically attractive predicting good approximations when the flow is not too complex. In short, the model explicitly gives the turbulent viscosity in term of the flow field and the distance from the wall, and hence, it has no mechanism to account for a high free stream turbulence level.

Among two equation turbulence models, well established two-equation models are developed to achieve a good prediction of flow field. The models considered here involve the low Reynolds k–ε models of Chien [11], Launder and Sharma [12], Biswas and Fukuyama [13], and two k–ω models by Wilcox including a standard version [14] without any near wall modification, and a transition version [15] specifically optimized to consider transition phenomenon. Wilcox has studied in detail the k–ω models, and classical low Re k–ε models in his book [16].

3.1 Baldwin–Lomax model

The Baldwin–Lomax model [10] is a two layer algebraic model for turbulent eddy viscosity term.

$$\mu_t = \begin{cases} \mu_{t_{\text{inner}}} & y \leqslant y_{\text{crossover}} \\ \mu_{t_{\text{outer}}} & y > y_{\text{crossover}} \end{cases} \tag{11}$$

$y_{\text{crossover}}$ is the minimum distance from the wall where $\mu_{t_{\text{inner}}}$ and $\mu_{t_{\text{outer}}}$ are equal.

$$y_{\text{crossover}} = \text{MIN}(y) : \mu_{t_{\text{inner}}} = \mu_{t_{\text{outer}}} \tag{12}$$

$\mu_{t_{\text{inner}}}$ is obtained by Prandtl–Van Driest model, where

$$\mu_{t_{\text{inner}}} = \rho l^2 |\Omega| \tag{13}$$

$$l = \kappa y (1 - \mathrm{e}^{-y^+/A^+}) \tag{14}$$

$$|\Omega| = \sqrt{2\Omega_{ij}\Omega_{ij}} \tag{15}$$

$$\Omega_{ij} = \frac{1}{2}\left(\frac{\partial u_i}{\partial x_j} - \frac{\partial u_j}{\partial x_i}\right) \tag{16}$$

$$\mu_{t_{\text{outer}}} = \rho K C_{c_p} F_{\text{wake}} F_{\text{kleb}}(y) \tag{17}$$

$$F_{\text{wake}} = \text{MIN}\left(y_{\max} F_{\max}; C_{wk} Y_{\max} \frac{U_{\text{dif}}^2}{F_{\max}}\right) \tag{18}$$

$F_{\max}$ and $y_{\max}$ are determined from the maximum of the function.

$$F(y) = Y|\Omega|(1 - \mathrm{e}^{-y^+/A^+}) \tag{19}$$

F_{kleb} is the intermittency factor given by:

$$F_{\text{kleb}}(y) = \left[1 + 5.5\left(\frac{y C_{\text{kleb}}}{y_{\max}}\right)^6\right]^{-1} \tag{20}$$

And U_{dif} is the difference between the maximum and minimum value of the velocity. For the boundary layer, the minimum value of the velocity is zero.

$$U_{\text{dif}} = \text{MAX}(\sqrt{u_i u_i}) - \text{MIN}(\sqrt{u_i u_i}) \tag{21}$$

Table 1 shows the value for constants in Baldwin–Lomax model.

Note that K is a constant here and must not be confused by turbulent kinetic energy. The free stream turbulent intensity does not appear in the model and is assumed zero.

3.2 k–ε models

The k–ε model used in this work is presented as

$$\frac{\partial}{\partial t}(\rho k) + \frac{\partial}{\partial x_j}\left[\rho k u_j - \left(\mu + \frac{\mu_t}{\sigma_k}\right)\frac{\partial k}{\partial x_j}\right] = P - \rho\varepsilon - \rho D \tag{22}$$

Table 1 Baldwin–Lomax constant

A^+	C_{cp}	C_{kleb}	C_{wk}	κ	K
26	1.6	0.3	0.25	0.4	0.0168

$$\frac{\partial}{\partial t}(\rho\varepsilon) + \frac{\partial}{\partial x_j}\left[\rho\varepsilon u_j - \left(\mu + \frac{\mu_t}{\sigma_\varepsilon}\right)\frac{\partial \varepsilon}{\partial x_j}\right] = (C_{\varepsilon 1} f_1 P - C_{\varepsilon 2} f_2 \rho\varepsilon)\frac{\varepsilon}{k} + \rho E \tag{23}$$

where, $C_{\varepsilon 1}$, $C_{\varepsilon 2}$, C_μ, σ_k, and σ_ε are the model constants, and f_1, f_2, and f_3 are the damping functions, and E and D are the source terms as shown in Table 2. The turbulent eddy viscosity μ_t and the turbulent kinetic energy production term, P, are:

$$\mu_t = C_\mu f_\mu \rho \frac{k^2}{\varepsilon} \tag{24}$$

$$P = \tau_{ij}^{\text{turb}} \frac{\partial u_i}{\partial x_j} \tag{25}$$

3.3 k–ω models

The k–ω models can be written in the general form of Eqs. (26–29). Various parameters of the models are given in Table 3

$$\frac{\partial}{\partial t}(\rho k) + \frac{\partial}{\partial x_j}\left[\rho k u_j - (\mu + \sigma^* \mu_t)\frac{\partial k}{\partial x_j}\right] = P - \beta^* \rho\omega k \tag{26}$$

$$\frac{\partial}{\partial t}(\rho\omega) + \frac{\partial}{\partial x_j}\left[\rho\omega u_j - (\mu + \sigma^* \mu_t)\frac{\partial \omega}{\partial x_j}\right] = \alpha\frac{\omega}{k}P - \beta\rho\omega^2 \tag{27}$$

$$\mu_t = \alpha^* \frac{\rho k}{\omega} \tag{28}$$

$$p = \tau_{ij}^{\text{turb}} \partial u_i / \partial x_j \tag{29}$$

The asymptotic behavior of ω approaching a wall is $\omega \sim 1/y^2$ as $y \to 0$. However, using a finite value of ω_{wall} is suitable from numerical point of view based on Wilcox's recommendation [16]. The surface roughness model gives a finite value for ω_{wall} as in Eqs. (15) and (16). If k_R^+, which is the nondimensional average sand–grain roughness height, is set to a value below 5 a hydraulically smooth surface is obtained, otherwise a k_R^+ value of 5 are used in all simulations presented here.

$$\omega_{\text{wall}} = u^{*^2} \times SR/\nu \tag{30}$$

where,

$$SR = \left\{ \begin{array}{l} (50/k_R^+)^2 \ldots\ldots\ldots\ldots k_R^+ < 25 \\ 100/k_R^+ \ldots\ldots\ldots\ldots\ldots k_R^+ \geqslant 25 \end{array} \right\} \quad k_R^+ = u^* k_R/\nu \tag{31}$$

4 Numerical method

Compressible Navier–Stokes equations are discretized using a non-uniform orthogonal grid generated by Stager–Sorenson elliptic differential equation. The inviscid flux terms are approximated by first order Roe method [18], and the viscous terms are approximated by second order gradient theorem. To prevent expansion shock, the entropy condition is used. The time integration is first order explicit Euler method. The time step is calculated from the CFL criterion using the local flow properties, which results variable time step throughout the flow field until achieving the steady state solution. The computational domain is shown in Fig. 1. The total number of grids used in this study is 32,000 which is fine enough to capture mean turbulent properties near the wall, that is, there are grid points within $0 < y^+ < 5$.

Table 2 k–ε model constant

	Chien	Launder–Sharma	Biswas–Fukuyama
C_μ	0.09	0.09	0.09
σ_k	1	1	1.4
σ_ε	1.3	1.3	1.3
D	$2\nu\frac{k}{y^2}$	$2\nu(\frac{\partial\sqrt{k}}{\partial y})^2$	0
E	$-\frac{2\nu\varepsilon}{y^2}e^{-0.5y^+}$	$2\nu\nu t(\frac{\partial^2 y}{\partial y^2})^2$	0
$C_{\varepsilon 1}$	1.35	1.44	1.46
$C_{\varepsilon 2}$	1.8	1.92	1.9
f_μ	$1 - e^{-0.0115y^+}$	$1 - e^{\frac{-3.4}{(1+R_t/50)^2}}$	$[1 - e^{(-Re_t/150)}][1 + 18.5/Re_t]$
f_1	1	1	$1 + 0.3e^{(-(Re_t/50)^2)}$
f_2	$1 - 0.22e^{-(\frac{Re_t}{6})^2}$	$1 - 0.3e^{-Re_t^2}$	$[1 - 0.3e^{(-(Re_t/6.5)^2)}][1 - e^{(-Re_y/10)}]$

$y^+ \equiv \frac{yu^*}{\nu}, Re_t = \frac{k^2}{\nu\varepsilon}, k_{\text{wall}} = 0, \varepsilon_{\text{wall}=0}, Re_y = \frac{\rho y\sqrt{k}}{\mu}$,

Table 3 k–ω model constant

	Standard version	Transition version
α^*	1	$\frac{\alpha_0^* + (Re_t/R_k)}{1+(Re_t/R_k)}$
α	$\frac{5}{9}$	$\frac{5}{9}\frac{\alpha_0 + (Re_t/R_\omega)}{1+(Re_t/R_\omega)}\frac{1}{\alpha^*}$
β^*	$\frac{9}{100}$	$\frac{9}{100}\cdot\frac{\frac{5}{18}+(Re_t/R_\beta)^4}{1+(Re_t/R_\beta)^4}$
β	$\frac{3}{40}$	$\frac{3}{40}$
σ^*	$\frac{1}{2}$	$\frac{1}{2}$
σ	$\frac{1}{2}$	$\frac{1}{2}$

$Re_t = \frac{\rho k}{\omega\mu}, \alpha_0^* = \frac{\beta}{3}, \alpha_0 = 1/10, R_\beta = 8, R_k = 6., R_\omega = 2.7$

4.1 Boundary condition

Temperature, stagnation pressure and the angle of attack are the conditions specified at the inlet. At the outlet, static pressure is identified. The values of k and ε at the inlet are calculated using the inlet conditions from the following equations.

$$k_1 = 3 \times Tu^2 U_1^2/2 \tag{32}$$

$$\varepsilon_1 = C_\mu^{3/4} k^{3/2}/l_m \tag{33}$$

$$\omega_1 = k^{1/2}/(\beta^* l_m) \tag{34}$$

At the solid wall, no slip boundary conditions and constant temperature are applied, and at the other boundaries, periodic boundary conditions are implemented.

4.2 Leading edge problem

In most of the k–ε and k–ω models, the condition at the stagnation point is not properly calculated and the turbulent kinetic energy is too high at this region. This is because, the Boussinesq assumption is not an accurate model to study flow around the stagnation point where the normal strain rate is large. This high turbulent kinetic energy generated around the stagnation point is transported to the boundary layer region. This problem may be resolved by modifying the turbulent kinetic energy in the k equation. This method originally suggested by Kato–Launder [19].

$$P_k = \mu_t S\Omega \tag{35}$$

where,

$$S = \sqrt{1/2\left(\frac{\partial u_i}{\partial x_j} + \frac{\partial u_j}{\partial x_i}\right)^2}, \quad \Omega = \sqrt{1/2\left(\frac{\partial u_i}{\partial x_j} - \frac{\partial u_j}{\partial x_i}\right)^2} \tag{36}$$

Another method is to modify the turbulent dissipation rate equation, which is applied only for k–ε equation. This modification, originally suggested by Yap [17], consists of an extra source term added to right hand side of the ε equation. Its effect is to reduce the departure of the near-wall length scale from its local equilibrium value. This does not influence the Launder–Sharma model very much, but the Chien model gives significantly better results close to the leading edge. Note that the Yap modification only affects the results close to the leading edge.

$$\rho S_\varepsilon = 0.83\rho\frac{\varepsilon^2}{k}\left(\frac{k^{1.5}}{\varepsilon l_e} - 1\right)\left(\frac{k^{1.5}}{\varepsilon l_e}\right) \tag{37}$$

where $l_e = c_\mu^{-0.75} \times 0.4y$

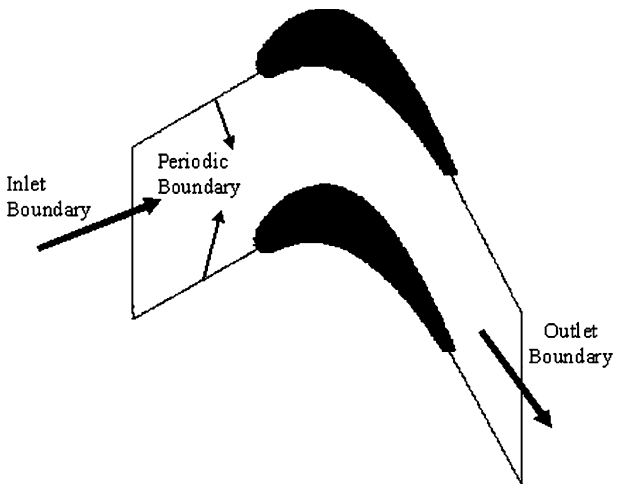

Fig. 1 Computational domain

5 Results and discussion

Direct numerical simulation of turbulence phenomena at high Reynolds number problems like turbine cascades is not a possible approach yet. Therefore, various turbulence models have been carried out to resolve these problems by incorporating experimental data available. Despite a lot of work in turbulence modeling, all of them still have deficient in predicting flow and heat transfer in a turbine cascade, especially on the suction side due to presence of various complicated phenomena consisting of the stagnation point, steep adverse and favorable pressure gradients, free stream turbulences, high Mach numbers, and 3D effects. None of the turbulence models can resolve all these phenomena in whole region by alone. Hence, the results obtained here employing different turbulence models

are still deficient especially on the suction side of the blade. Following, the performance of six turbulence models in predicting heat transfer over the VKI turbine blade is compared with the experimental data available.

5.1 Zero equation model (Baldwin–Lomax model)

Two cases with different Reynolds numbers are examined here. When the turbulent eddy viscosity is 14 times greater than molecular viscosity at the inlet, $\mu_t \geq 14*\mu_1$, the flow is assumed turbulent.

Case 1: The flow properties in this case are $M_{2is} = 1.12$, $Re_{2is} = 1.05 \times 10^6$, $I = -5°$ and $T_0 = 420$ K. In Fig. 2, the numerical results and experimental data [5] available for two free stream turbulent intensities, i.e. 4 and 0.8% are compared. The figure shows the heat transfer distribution as a function of coordinate measured along the suction side (positive values) and the pressure side (negative values). Since the Baldwin–Lomax (BL) model does not involve free stream turbulent intensity, the results are in better agreement with the experimental data when the free stream turbulent intensity is low. On the suction side of the blade, the flow remains laminar up to $S \cong 0.08$ m, but on the pressure side, the flow is turbulent throughout.

Case 2: The flow properties used in this case are:

$M_{2is} = 1.12$, $Re_{2is} = 0.54 \times 106$, $I = -5°$ and $T_0 = 420$ K. Figure 3 shows the heat transfer at the wall. As shown, the result at the suction side is in good agreement with the experimental data [20] except near the trailing edge due to separation of the flow, but in the pressure side of the blade, the results indicate underestimation and laminar flow over whole region. The reason is that in BL model the free stream turbulent intensity is not taken into account. In this case, at the suction side, the flow is laminar up to $S \cong 0.1$ m.

5.2 Two equation models

Two different corrections consisting of Kato–Launder and Yap corrections are taken into account for well predicting leading edge problem. First, various turbulent length scales are examined to determine an optimum value for better approximation in comparison with experimental data. The length scale used in the three k–ε models is 0.05 of pitch value, and in two k–ω models is 0.005 of pitch value. In all cases, the turbine blade is considered as RS1S[20] profile (VKI) with the following geometric specifications

$\alpha_2 = -65°$, $\alpha_1 = 53.36°$, $\gamma = 58.38°$, $g/c = 0.7607$, $c = 71.81$ mm

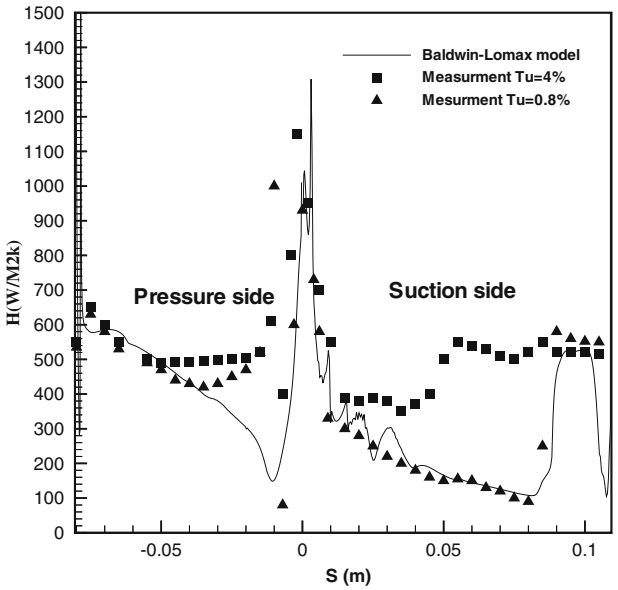

Fig. 2 Heat transfer distribution ($M_{2is} = 1.12$, $Re_{2is} = 1.05e6$, $I = -5°$, $T_u = 4\%$)

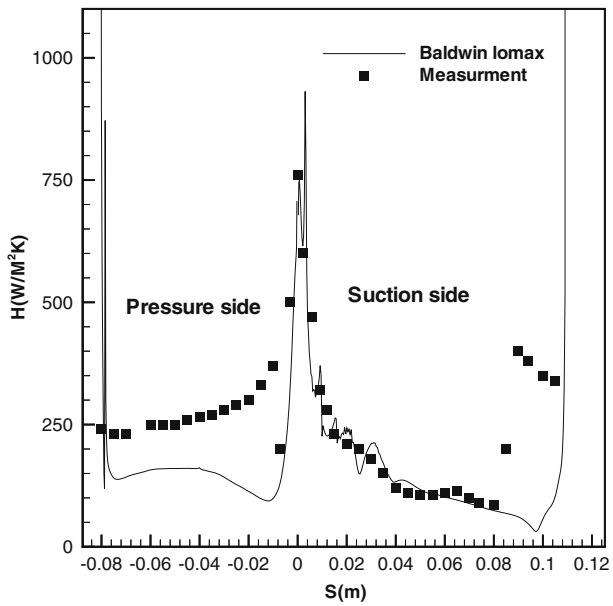

Fig. 3 Heat transfer distribution ($M_{2is} = 1.12$, $Re_{2is} = 0.54e6$, $I = -5°$, $T_u = 4\%$)

Case 3: The flow properties in this case are $M_{2is} = 1.12$, $Re_{2is} = 1.05 \times 10^6$, $I = -5°$ and $T_0 = 420$ K. Figure 4 shows the heat transfer distribution as a function of the coordinate measured along the suction (positive values) and pressure sides (negative values) obtained with five different two equation models. Based on the experiments, the boundary layer on the suction side is laminar up to $S \approx 35$ *mm*, where

transition starts. As it is evident from the figure, all turbulence models except Wilcox LRN (low Reynolds number) [15] are not able to capture accurately this laminar region. Beyond the laminar region of the suction side in transition and fully turbulent boundary layer region, all turbulence models have a good trend in comparison with experimental data. The existence of a small recirculation bubble at the beginning of the pressure surface is proven by the strong heat transfer coefficient variation, indicating the separation and reattachment of the flow. The amplitude of this variation is strongly reduced by increasing turbulent intensity (Figs. 4 and 9). At the pressure side, the Launder–Sharma [12] model indicates a better approximation comparing with the experimental data than the other models due to well capturing of the immediate transition in the leading edge.

Cases 4 and 5: To investigate the effect of Reynolds number, the following properties are used $M_{2is} = 1.12$, $T_u = 4\%$, $I = -5°$, $T_0 = 420$ K, with Reynolds number of $Re_{2is} = 0.54 \times 10^6$ and $Re_{2is} = 1.84 \times 10^6$ for cases 4 and 5, respectively. Heat transfer coefficient distribution at the wall of the blade is indicated in Fig. 5. On the suction side, the Launder–Sharma [12] and Biswas–Fukuyama [13] and LRN Wilcox [15] models are able to capture the laminar region, but the other models [11, 14] studied here predict an almost immediate transition at the leading edge and a fully turbulent boundary layer over the whole suction side. In addition, it can be realized that the transition locations predicted by LRN Wilcox [15] and Launder–Sharma [12] are physically correct, but Biswas–Fukuyama [13] model is not able to predict transition location correctly. Overall, LRN Wilcox [15] model is able to well predict whole suction side of the blade. On the pressure side Launder–Sharma [12] model has a better approximation comparing with experimental data than the other models. By comparing the numerical results obtained, it can be concluded that the k–ω models predict suction side better than pressure side and this is reverse for the k–ε models. The reason stems from the well prediction of separation region on the suction side of the turbine blade by the k–ω models. In Fig. 6, the effect of increasing Reynolds number in heat transfer approximation is represented. In this case, because of turbulent flow over whole pressure and suction side of the blade, all turbulence models indicate better results comparing with experimental data than the low Reynolds number cases (Fig. 5). As shown in this figure, transition is captured at the suction side by the three models including LRN Wilcox, Biswas–Fukuyama and Launder–Sharma, however, the other two models (Chiens and HRN Wilcox) are not able to predict the transition region. The comparison of Figs. 4, 5, 6 indicates that due to increase of Reynolds number, the heat transfer coefficient increases. Also, transition location on the suction side moves to the leading edge as the Reynolds number decreases, which is in good agreement with the measurement.

Case 6,7: In these cases including case 3 the effect of free stream Mach number are studied, where the flow parameters are $Re_{2is} = 1.05 \times 10^6$, $I = -5°$, $T_0 = 420$ K and $T_u = 4\%$. The Mach numbers are 0.795 and 1.277 for cases 5 and 6, respectively. Figure 7

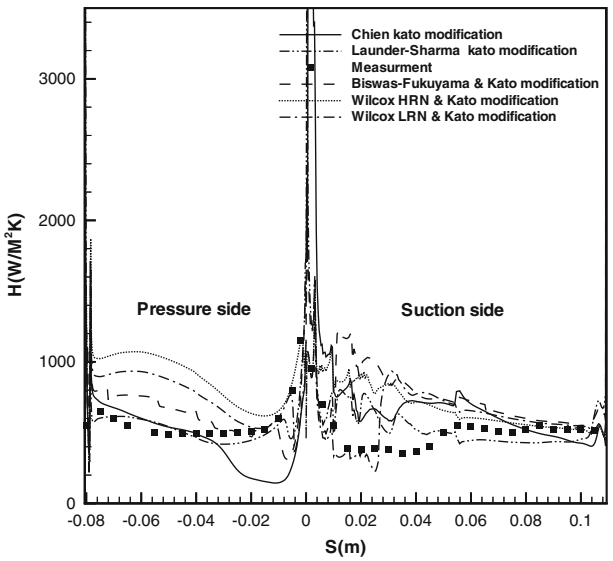

Fig. 4 Heat transfer distribution ($M_{2is} = 1.12$, $Re_{2is} = 1.05e6$, $I = -5°$, $T_u = 4\%$)

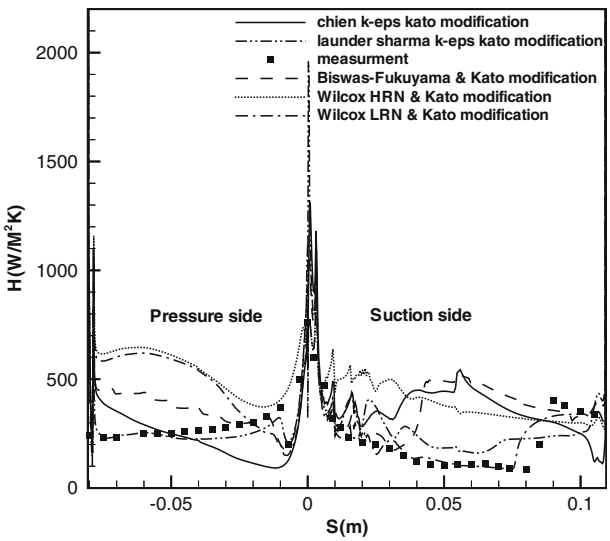

Fig. 5 Heat transfer distribution ($M_{2is} = 1.12$, $Re_{2is} = 0.54e6$, $I = -5°$, $T_u = 4\%$)

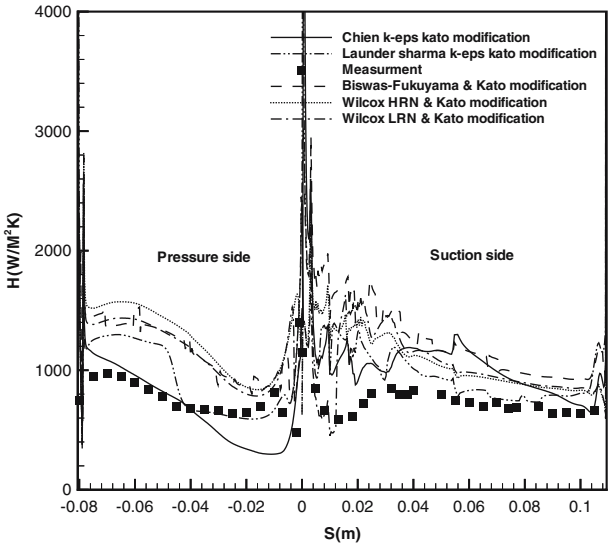

Fig. 6 Heat transfer distribution (M_{2is} = 1.12, Re_{2is} = 1.84e6, I = –5°, T_u = 4%)

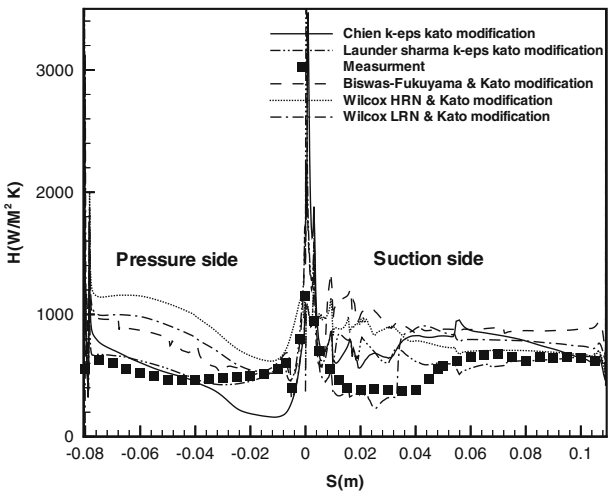

Fig. 7 Heat transfer distribution (M_{2is} = 0.795, Re_{2is} = 1.05e6, I = –5°, T_u = 4%)

shows heat transfer coefficient distribution on the blade surface for the five two equation models presented here along with the experimental data of Arts et al. [20]. The comparison of the results of two different Mach numbers indicate that the heat transfer coefficient distribution on the pressure side are the same quantitatively and qualitatively, but on the rear part of suction side of the blade increasing Mach slightly reduces the heat transfer coefficient. This is due to interaction of shock and boundary layer at supersonic Mach numbers (Figs. 4, 8).

Case 8: The purpose of this case is to study the effect of turbulence intensity on the heat transfer coefficient.

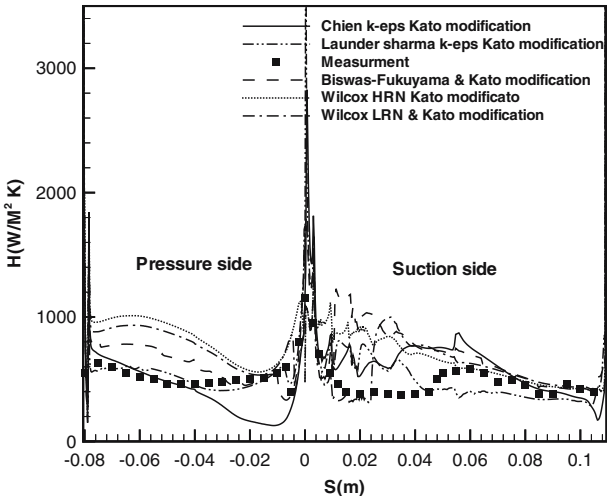

Fig. 8 Heat transfer distribution M_{2is} = 1.277, Re_{2is} = 1.05e6, I = –5°, T_u = 4%)

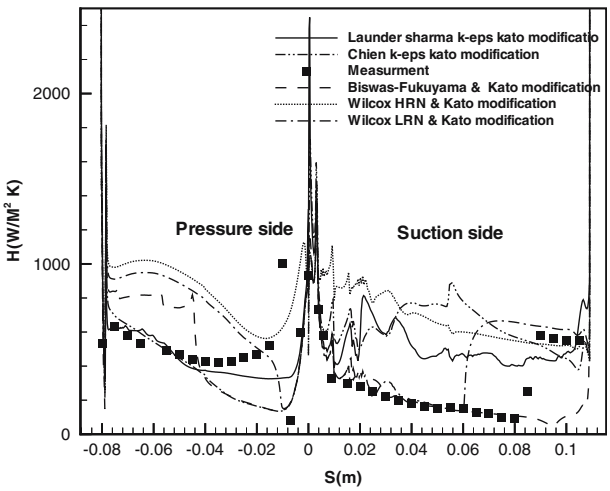

Fig. 9 Heat transfer distribution (M_{2is} = 1.12, Re_{2is} = 1.05e6, I = –5°, T_u = 0.8%)

Here, flow conditions are M_{2is} = 1.12, Re_{2is} = 1.05 × 10^6, I = –5°, T_0 = 420 K, and T_u = 0.8%. The results of this case and case 3 are used to compare the turbulent intensity effect. In Fig. 9, heat transfer distribution coefficient for five turbulence models presented here are shown for lower intensity of 0.8%. Comparing Figs. 4 and 9 indicates that for higher turbulent intensity flows, the numerical results are closer to experimental data than lower intensity ones. This is due to better physical behavior of turbulence models at higher intensity flows.

Cases 9,10: In these both cases, the performance of Yap correction is investigated in two k–ε models. The flow parameters are M_{2is} = 1.12, I = –5°, T_0 = 420 K and T_u = 4%. For case 9, Re_{2is} =

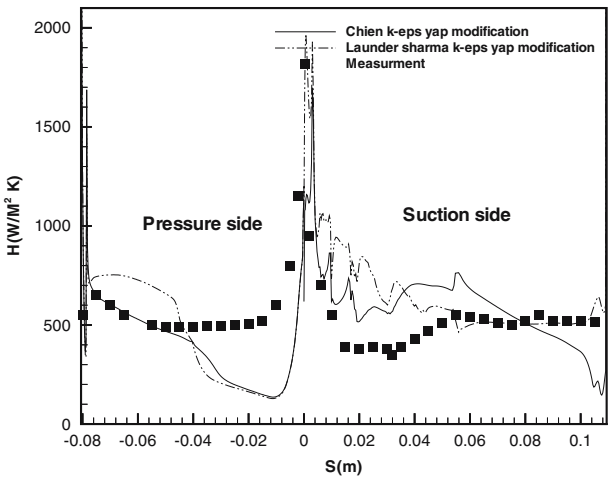

Fig. 10 Heat transfer distribution (M_{2is} = 1.12, Re_{2is} = 1.05e6, I = –5°, T_u = 4%)

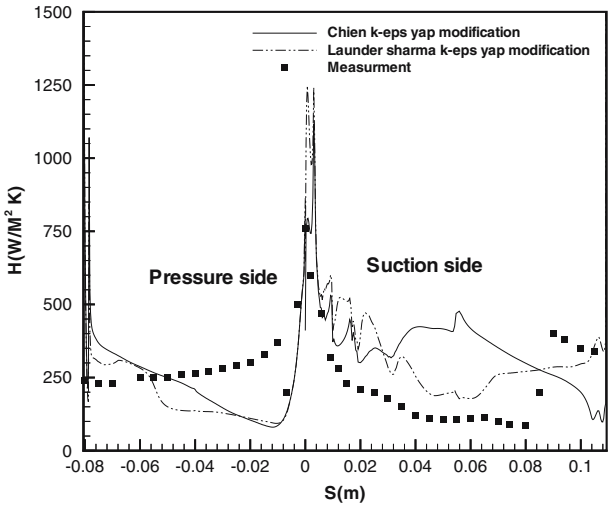

Fig. 11 Heat transfer distribution (M_{2is} = 1.12, Re_{2is} = 0.54e6, I = –5°, T_u = 4%)

1.05×10^6% and for case 10, $Re_{2is} = 0.54 \times 10^6$. The results are shown in Figs. 10 and 11. The correction made in both cases indicate that the heat transfer rate at the leading edge is calculated more accurately comparing with the results of Kato correction indicated in Figs. 4 and 5. But in the other regions the Kato correction results predicts better heat transfer rates.

6 Conclusion

To investigate heat transfer over the VKI turbine blade, a finite volume method is employed to solve governing equations using six different turbulence models including the algebraic Baldwin–Lomax [10], three low-*Re* k–ε models [1–3], and two k–ω models [4].

All two equation models used are based on the Boussinesq assumption and predict too high turbulence levels in the stagnation region. The k–ε models, especially the Chien model, are much more affected by stagnation point than the k–ω models, predicting a very large value for the heat transfer coefficient. The effect of turbulent intensity is studied and it is indicated in the all of models with increase of free stream turbulent intensity, heat transfer rate increases. Predicted transition point only in Wilcox LRN k–ω and Biswas–Fukuyama k–ε models are affected by free stream turbulent intensity causing the transition point move to the leading edge at the suction side. None of the models except Biswas–Fukuyama k–ε [13] and Wilcox LRN k–ω models [15] tested are able to predict transition and any laminar region presence at the suction side. The k–ω models are numerically easier to implement and work better in the leading edge.

As the Reynolds number and free stream turbulent intensity increases, the approximation of heat transfer by turbulence models becomes better comparing experimental data. However, variation of Mach number at constant Reynolds numbers does not have any considerable effect on heat transfer rate except a very slight reduction in heat transfer on rear part of suction side for large Mach numbers.

Lastly, the main point should be mentioned here is that because of complicated flow field in turbine cascades, still there is not any turbulence model to well predict heat transfer rate over entire suction and pressure side of turbine blade.

References

1. Thole KA, Bogard DG (1995) Enhanced heat transfer due to high free stream turbulence. ASME J Turbomach 117:418–424
2. Maciejewski PK, Moffat RJ (1992) Heat transfer with very high free-stream turbulence: Part I and II. ASME J Heat Transf 114:827–839
3. Dullenkopf K, Schultz A, Wittig S (1991) The effect of a incident wake conditions on the mean heat transfer of and airfoil. ASME J Turbomach 113:412–418
4. Magari PJ, Lagraff LE (1994) Wake–induced unsteady stagnation-region heat transfer measurements. ASME J Turbomach 116(1):29–38
5. Rao KV, Delaney RA, Dunn MG (1994) Vane–blade interaction in a transonic turbine. J Propuls Power 10(3):305–317
6. Blair MF (1994) An experimental study of heat transfer in a large-scale turbine rotor passage. ASME J Turbomach 10(1):1–13

7. Boyle RJ (1992) Navier-Stokes analysis of turbine blade heat transfer. ASME J Turbomach 113(3):392–403
8. Ameri AA, Sockol PM, Gorla RSR (1992) Navier–Stokes analysis of turbomachinery blade external heat transfer. J Propuls Power 8(2):374–381
9. Daniels LD, Browne WB (1981) Calculation of heat transfer rates to gas turbine blades. Int J Heat Mass Transf 24(5):871–879
10. Baldwin, Lomax (1978) Thin layer approximation and algebraic model for separated turbulent flow. AIAA paper 78–257
11. Chien K-Y (1982) Predictions of channel and boundary-layer flows with a low-Reynolds number turbulence model. AIAA J 20(1):33–38
12. Launder BE, Sharma BI (1974) Application of the energy-dissipation model of turbulence to the calculation of flow near a spinning disc. Lett Heat Mass Transf 1(2):131–138
13. Biswas D, Fukuyama Y (1994) Calculation of transitional boundary layers with an improved low Reynolds number version of the k–ε turbulence model. J Turbomach 116:765–773
14. Wilcox DC (1988) Reassessment of the scale determining equation for advanced turbulence model. AIAA J 26(11):1299–1310
15. Wilcox DC (1994) Simulation of transition with a two equation turbulence model. AIAA J 32(2):247–255
16. Wilcox DC (1993) Turbulence Modeling for CFD. DCW Industries Inc. La Canada, California
17. Yap CJ (1987) Turbulent heat and momentum transfer in recirculating and impinging flows, PhD Thesis, Faculty of Technology, University of Manchester
18. Roe PL (1981) Approximate Riemann solvers, parameter vectors and difference schemes. J Comput Phys 43(2):357–372
19. Kato M, Launder BE (1993) The modeling of turbulent flow around stationary and vibrating square cylinders. In: Proceedings of ninth symposium on turbulent shear flow, Kyoto, pp 10.4.1–10.4.6
20. Arts T (1998) Aero thermal performance measurement and analysis of a two-dimensional high turning rotor blade. ASME J Turbomach 120:494–499